

PC-SNN: Predictive Coding-based Local Hebbian Plasticity Learning in Spiking Neural Networks

Haidong Wang^a, Xiaogang Xiong^b, Mengting Lan^b, Yinghao Chu^c, Zixuan Jiang^b, KC Santosh^d, Shimin Wang^e, Renxin Zhong^{a,*}

^a*School of Intelligent Systems Engineering, Sun Yat-Sen University (Shenzhen Campus), Guangdong, China.*

^b*School of Mechanical Engineering and Automation, Harbin Institute of Technology Shenzhen, Guangdong, China.*

^c*Department of Advanced Design and Systems Engineering, City University of Hong Kong, Hong Kong SAR.*

^d*Department of Computer Science, The University of South Dakota, SD, USA.*

^e*Department of Advanced Manufacturing Systems, Massachusetts Institute of Technology, MA, USA.*

Abstract

Spiking Neural Networks (SNNs), regarded as the third generation of neural networks, emulate the brain's information processing with unparalleled biological plausibility compared to traditional neural networks. However, their non-linear, event-driven dynamics pose significant challenges for training, and existing methods often deviate from neuroscientific principles of cortical learning. Drawing inspiration from predictive coding theory—a leading model of brain information processing—we propose PC-SNN, a novel learning framework that integrates predictive coding with SNNs to enable biologically plausible, local Hebbian plasticity without reliance on backpropagation. Unlike conventional SNN training approaches, PC-SNN leverages only local computations, aligning with the brain's distributed processing and overcoming the biological implausibility of global error propagation. Our classification model achieves competitive performance on the benchmark datasets, including Caltech Face/Motorbike, MNIST, and CIFAR10, surpassing state-of-the-art multi-layer SNNs. Furthermore, our predictive coding-based regression model outperforms backpropagation-based methods while adhering to local plasticity constraints, offering a scalable and biologically grounded alternative for SNN training. PC-SNN drives progress in neuromorphic computing through validating the adaptability of bio-inspired algorithms within spiking neural architectures, but also unveils novel understandings of neurocognitive learning processes, presenting a conceptual framework distinguished by its theoretical originality and functional efficacy.

Keywords: Spiking neural network, predictive coding, event camera, local Hebbian plasticity.

1. Introduction

Spiking Neural Networks (SNNs), often referred to as third-generation neural networks, are composed of bio-inspired spiking neurons that communicate via binary spikes, closely mimicking the event-driven processing of human biological neural systems (Maass, 1997). Renowned for their energy efficiency and

*Corresponding author.

Email addresses: hdwang26@mail2.sysu.edu.cn (Haidong Wang), xiongxg@hit.edu.cn (Xiaogang Xiong), 20s053097@stu.hit.edu.cn (Mengting Lan), yinghchu@cityu.edu.hk (Yinghao Chu), 190710110@stu.hit.edu.cn (Zixuan Jiang), kc.santosh@usd.edu (KC Santosh), bellewsm@mit.edu (Shimin Wang), zhrenxin@mail.sysu.edu.cn (Renxin Zhong)

biological plausibility, SNNs have demonstrated remarkable results on various tasks, particularly with event-driven data. These attributes make SNNs a promising paradigm for neuromorphic computing and neuroscience-inspired artificial intelligence. However, despite their potential, current SNN training methods often rely on techniques adapted from artificial neural networks (ANNs), which neglect the neuroscientific principles of cortical learning (Rao and Ballard, 1999; Lillicrap et al., 2020, 2016; Caucheteux et al., 2023). This reliance introduces a significant gap, as such methods fail to fully exploit the biological fidelity of SNNs, limiting their scalability and alignment with neural mechanisms.

The non-differentiable nature of SNNs makes training challenging with popular and well-studied gradient descent methods. Here are three major approaches to train SNNs. First, the spike-timing-dependent plasticity (STDP) learning algorithm provides a biologically inspired learning rule for SNNs by adjusting the relative spike timing between pre-synaptic and post-synaptic neurons, but the STDP approach may face difficulties with large-scale and complex tasks (Mozafari et al., 2018a; Kheradpisheh et al., 2018; Liu et al., 2021b). Second, the ANN-SNN conversion approach aims to convert well-established ANN architectures to SNNs, benefiting from the high performance of ANNs and the energy efficiency of SNNs (Roy et al., 2019; Han and Roy, 2020a; Jiang et al., 2023). However, this approach has several drawbacks, including information loss and performance degradation. Third, the surrogate gradient-based direct learning approach addresses some limitations of the ANN-SNN conversion approach by enabling end-to-end training using surrogate gradients to approximate gradients during training (Guo et al., 2022; Zenke and Ganguli, 2018). This approach achieves competitive accuracy compared to other methods and offers the flexibility to train a wide range of network architectures. However, the above studies on SNN training are all based on the backpropagation paradigm. Previous research has shown that feedback connections in the cerebral cortex do not exhibit the form of backpropagation (Rao and Ballard, 1999; Lillicrap et al., 2020, 2016), and the nature of SNNs mimic the information encoding and processing of the human brain by using discrete events to simulate the propagation of pulse signals. Therefore, studying biological plausibility and brain-like learning mechanism in SNNs holds great significance (Aceituno et al., 2023; Caucheteux et al., 2023).

The predictive coding theory, an influential theory in neuroscience, exhibits valuable intriguing properties within the learning and perception in the brain (Rao and Ballard, 1999; Friston, 2003, 2005; Ororbia et al., 2024; Salvatori et al., 2023). It has developed various approaches to approximate backpropagation in non-spiking multilayer perceptron (MLP) networks models using biologically plausible connectivity schemes and Hebbian learning rules (Bengio and Fischer, 2015). Whittington and Bogacz demonstrated that the predictive coding framework, a biologically feasible hierarchical process derived from a probabilistic model, can achieve effects similar to backpropagation in ANNs (Whittington and Bogacz, 2017; Rao and Ballard, 1999; Friston, 2003, 2005). The predictive coding model introduces additional nodes to compute local prediction errors between the values of random variables at a given layer and those assessed by lower layers. Moreover, mechanisms consistent with this prediction error propagation have been observed during perceptual decision tasks (Summerfield et al., 2006, 2008).

In this work, we propose a framework to effectively integrate predictive coding into SNNs across various tasks, offering distinct advantages. First, we develop a predictive coding spiking neural network (PC-SNN) for image classification that leverages local Hebbian plasticity. Second, we implement a predictive-coding-through-time (PCTT) learning algorithm within an adaptive spiking recurrent neural network (ASRNN) for predicting angular velocities from event camera data. Our results demonstrate excellent performance across these tasks. Compared to conventional SNN training methods, our Hebbian-inspired predictive coding approach is not only biologically plausible but also incorporates neurobiological constraints typically overlooked in artificial systems:

- We proposed PC-SNN and ASRNN with PCTT, achieving state-of-the-art performance on classifica-

tion and regression tasks on both traditional image and event camera datasets.

- The predictive coding mechanism in SNNs achieves the basis for brain-like local computation and local plasticity, wherein neurons execute computations based solely on the activity of their input neurons and the synaptic weights associated with these inputs, rather than relying on information encoded elsewhere in the neural network. Additionally, synaptic plasticity is determined exclusively by the activity of presynaptic and postsynaptic neurons.

2. Related Work

2.1. Spiking Neural Network training Methods

Compared to the rapid development of ANNs, SNNs training algorithms remain an active area of research due to their inherently non-differentiable nature. In general, SNN training algorithms fall into three categories: STDP based localized learning rules (Bi and Poo, 1998; Liu et al., 2021b; Mozafari et al., 2018a; Kheradpisheh et al., 2018; Liu et al., 2021b), ANN-SNN conversion methodologies (Roy et al., 2019; Han and Roy, 2020a; Jiang et al., 2023), and surrogate gradient-based direct learning approach (Guo et al., 2022; Zenke and Ganguli, 2018). Unsupervised and semi-supervised learning algorithms based on STDP are limited to shallow SNNs, often underperforming compared to ANNs on complex datasets. The top-performing SNNs, usually made of Integrate-and-Fire (IF) neurons, are created through ANN-SNN transformations by training non-spiking ANNs with ReLU activation functions. To deepen these networks, spike-based error backpropagation algorithms have been proposed for supervised SNN training.

Mostafa (2017) proposed a feedforward spiking network that implements a temporal coding scheme using spike times as the information preserver instead of sparse spike counts. They developed a direct training approach that does not require spiking networks to degenerate to conventional ANNs. By establishing a linear and differentiable relation between any given spike time and all spikes that have an impact on it in the z -domain, any differentiable cost function related to network spike times can be imposed through gradient descent verification. Kheradpisheh and Masquelier (2020) proposed a novel supervised learning algorithm named S4NN for multi-layer SNNs. It encodes input spikes such that spiking latency is inversely proportional to pixel value, enabling rapid and accurate decision-making with minimal spikes. Using rank-order coding, each neuron fires at most one spike per stimulus. Additionally, S4NN introduces relative target firing time to ensure correct output neuron activation and approximates ReLU using IF neurons

2.2. Biological plausibility

Spike-based error backpropagation algorithms adjust the strength of synapses/weights to minimize errors by backpropagating them through feedback networks. However, Zipser and Rumelhart (1993) questioned whether a similar adaptive mechanism exists in biological neural systems. Neuroscientists generally agree that there is no evidence of backpropagation occurring in biological nervous systems, primarily because such systems lack the specialized feedback networks that are integral to backpropagation algorithms but not found in biological neural systems (Crick and Francis, 1989). Additionally, it is challenging to establish a one-to-one correspondence between synapses in feedforward and feedback networks or to adapt the strengths of corresponding connections during learning, as most connections between neurons involve multiple synapses. Lin (2021) proposed a feedback-network-free algorithm for SNNs that is both essentially and mathematically equivalent to the traditional backpropagation algorithm. This novel approach is inspired by retrograde regulatory mechanisms believed to exist in neurons and eliminates the need for a feedback network, thereby significantly enhancing the biological plausibility of learning capabilities in neural networks.

Several models have been introduced in ANN learning algorithms that aim to implement backpropagation in multi-layer perceptron MLP-style models using only biologically plausible connectivity schemes and Hebbian learning rules. [Whittington and Bogacz \(2017\)](#) demonstrated that the backpropagation algorithm can be closely approximated by employing a simple local Hebbian plasticity rule, which involves only the activities of presynaptic and postsynaptic neurons directly connected to the synapse being modified during learning. Inspired by the predictive coding framework ([Rao and Ballard, 1999](#); [Friston, 2003, 2005](#)), their proposed model suggests that this form of inference could be implemented by biological neural networks.

[Millidge et al. \(2020\)](#) recently demonstrated a strong correlation between predictive coding theory and automatic differentiation across arbitrary computation graphs, achieving the desired outcome on three mainstream machine learning architectures (CNNs, RNNs, and LSTMs). They utilized a predictive coding framework with local learning rules and mostly Hebbian plasticity. [Ororbia and Mali \(2023\)](#) applied predictive coding to convolution-based computations using a flexible neurobiologically inspired algorithm that iteratively refines latent state feature maps to construct accurate internal representations of images. Several investigations in the domain of convolutional-based SNNs have shown exceptional results, including ANN-SNN, Surrogate Gradient, Direct Training among others attaining state-of-the-art performance on challenging datasets such as CIFAR and ImageNet ([Han et al., 2020](#); [Li et al., 2021](#); [Yao et al., 2023](#); [Li et al., 2022](#)). [Song et al. \(2020\)](#) presented a brain learning model that achieves local plasticity and full autonomy through the use of a fully autonomous Z-IL (Fa-Z-IL) model. This model is equivalent to BP but does not require any control signal, allowing for simultaneous and autonomous computation at the local level. However, there is currently no formulation available for a biologically plausible predictive coding SNN with local Hebbian synaptic plasticity that draws inspiration from neuroscience.

3. Preliminaries

In this section, we introduce the fundamental concepts of our spiking neural network framework, including first-spike temporal coding, spiking neuron model, dynamic target firing time, and backpropagation-based training. These concepts form the theoretical foundation for our proposed predictive coding framework.

3.1. First-spike temporal coding

We use a sparser temporal coding strategy that encodes the firing time of neurons, rather than the analog output of an ANN neuron through spiking rates. Specifically, each neuron can only be activated once within a predefined time interval and those neurons that fire first are considered the most active. To encode input images into spike trains, we denote the i^{th} pixel value as P_i in grayscale images with pixel values ranging from $[0, P_{\max}]$. The larger the pixel value, the earlier it fires. To convert pixel values to firing times within $[0, t_{\max}]$, we use this linear transformation formula:

$$t_i = \frac{P_{\max} - P_i}{P_{\max}} t_{\max}. \quad (1)$$

Subsequently, the input spike trains of the i^{th} pixel (denote input layer as layer 0) can be represented as follows:

$$S_i^0(t) = \begin{cases} 1 & \text{if } t = t_i \\ 0 & \text{otherwise} \end{cases} \quad (2)$$

Neurons in the hidden layers and output layer integrate incoming spikes over time with no leakage, emitting only one spike when their membrane potentials cross the threshold for the first time. If a neuron's potential

never reaches the threshold, it remains silent. During training, it is necessary to determine the firing time of all neurons. Therefore, if a neuron fails to reach threshold during training, we artificially set its activation time to t_{max} .

3.2. Spiking neurons model

We integrate neurons' potential and stimulate them without leakage by accumulating received spikes from presynaptic neurons through dendritic connections. Each presynaptic spike corresponds to a synaptic weight that raises the neuron's potential during integration. Neurons emit signals when their internal potentials reach a predefined threshold. The membrane potential of the j^{th} neuron in the l^{th} layer is described as follows:

$$V_j^l(t) = \sum_i w_{ji}^l \sum_{\tau=1}^t S_i^{l-1}(\tau) \quad (3)$$

where w_{ji}^l signifies the synaptic weight between the i^{th} presynaptic neuron and the j^{th} neuron in l^{th} layer; and $S_i^{l-1}(\tau)$ denotes the spike train of the i^{th} presynaptic neuron in layer $l-1$.

If $V_j^l(t)$ transcends its threshold, then the neuron emits a spike:

$$S_j^l(t) = \delta(t - t_j^l) = \begin{cases} 1 & \text{if } V_j^l(t) \geq \theta_j^l \wedge S_j^l(< t) \neq 1 \\ 0 & \text{otherwise} \end{cases} \quad (4)$$

where $S_j^l(< t) \neq 1$ means that the neurons do not fire until time t .

3.3. Dynamic target firing time

One of the common methods for setting the target firing time is using fixed firing time: assuming that we have C categories of input images and the label of one input image is i , then the target firing time of the i^{th} neuron in the output layer is set to $T_i^o = \tau$, where τ is a given constant. The activation time of the remaining output neurons is set to $T_j^o = t_{max}$, $1 \leq j \leq C$, $j \neq i$. Although the above setting method is simple and easy to implement, when the actual firing time of the i^{th} neuron $t_i^o < \tau$, this setting affects the response speed of the network and can not meet our expectation of having the network respond as quickly as possible.

In this paper, we followed the dynamic target firing time proposed by S4NN model (Kheradpisheh and Masquelier, 2020) which takes the actual activation time into account. Assuming that we feed the image of i^{th} category to the network, the first step is to obtain the actual minimum activation time of the output neuron: $\tau = \min\{t_j^o \mid 1 \leq j \leq C\}$, then the dynamic target firing time of the j^{th} output neuron is set as follows:

$$T_j^o = \begin{cases} \tau & \text{if } j = i \\ \max\{\tau + \gamma, t_j^o\} & \text{if } j \neq i \end{cases} \quad (5)$$

where $\gamma > 0$ is a constant.

In the above setting of dynamic target firing time, the output neuron of the true category is set to the minimum firing time. The positive constant γ ensures the minimum distance between the firing time of the true category neuron and that of the remaining neurons. Neurons whose activation times are much later than τ do not change their values.

3.4. SNN trained with backpropagation

To demonstrate the theoretical advantages of PC-SNN over BP-SNN in terms of bio-plausibility, we will briefly review the SNN temporal-coding-based backpropagation algorithm in this section. For a C -category classification task, we define a temporal mean square error function as follows:

$$L = \frac{1}{2} \sum_{j=1}^C (t_j^o - T_j^o)^2 \quad (6)$$

where t_j^o and T_j^o represent the actual and targeted firing time of the j^{th} output neuron respectively. Let's define an intermediate gradient as $\delta_j^l = \frac{\partial L}{\partial t_j^l}$. Therefore backpropagation (BP) updates the weights of the SNN by:

$$\Delta w_{ji}^l = -\eta \frac{\partial L}{\partial w_{ji}^l} = -\eta \frac{\partial L}{\partial t_j^l} \frac{\partial t_j^l}{\partial w_{ji}^l} = -\eta \delta_j^l \sum_{\tau=1}^{t_j^l} S_i^{l-1}(\tau) \quad (7)$$

where $\frac{\partial t_j^l}{\partial w_{ji}^l} = \sum_{\tau=1}^{t_j^l} S_i^{l-1}(\tau)$ is formulated detailedly in (Kheradpisheh and Masquelier, 2020). The intermediate signal is given as follows:

$$\delta_j^l = \begin{cases} t_i^o - T_i^o & \text{if } l=o \\ \sum_k \delta_k^{l+1} w_{kj}^{l+1} [t_j^l \leq t_k^{l+1}] & \text{if } l \in \{1, \dots, l_{\max}-1\} \end{cases}$$

where $l = l_{\max}$ when $l = o$. An example of a two-layer BP-trained SNN (BP-SNN) is shown in Fig. 1(A). It's important to construct a feedback structure in order to backpropagate the intermediate gradient signal from δ_k^{l+1} to δ_j^l . This means that the weights of the feedback network must correspond with those of the feed-forward network.

4. Method

In this section, we present our novel learning framework for SNNs, which incorporates predictive coding and local Hebbian synaptic plasticity mechanisms for both classification and regression tasks.

4.1. PC-SNN for Classification

4.1.1. Encoding strategy

During SNN training, the pixel intensities of images can be converted to spikes by multiple strategies. We use a Time-To-First-Spike time-based (TTFS) coding strategy (Rathi et al., 2020) that encodes the firing time of neurons, rather than the analog output of an ANN neuron through spiking rates. Specifically, each neuron can only be activated once within a predefined time interval, and those neurons that fire first are considered the most active. In short, the larger the pixel value, the earlier the spike fires.

4.1.2. Neuron Dynamics

We integrate the potentials of neurons in the hidden and output layers by accumulating received spikes from presynaptic neurons through dendritic connections without leakage. Each presynaptic spike corresponds to a synaptic weight that raises the neuron's potential during integration, leading to the emission of signals when the internal potential reaches a predefined threshold. If a neuron's potential does not reach the

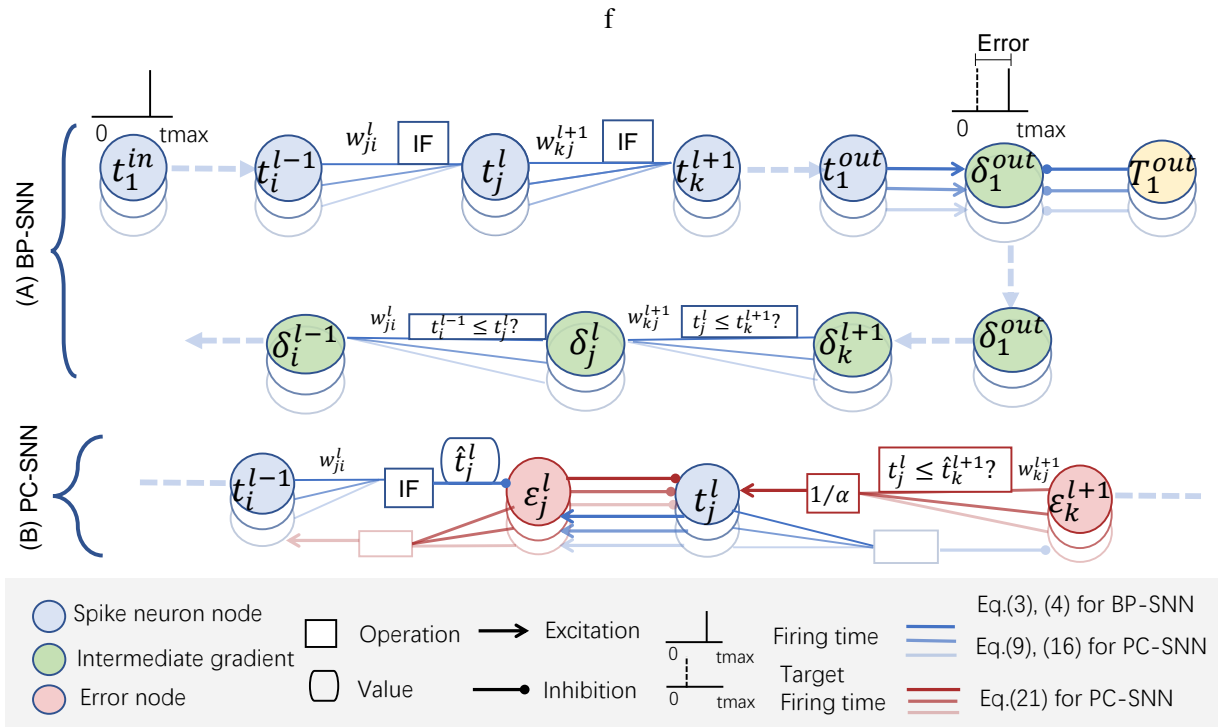


Figure 1: (A): SNN trained with BP (BP-SNN). This is a two-layer spiking neural network. Input layer encodes the pixel values into spike trains by temporal encoding. IF neurons in the hidden and output layer transmit information by processing the received spike train and responding to it. Backpropagation compares the actual firing time obtained by the output layer with the target firing time, and propagates the gradient backward layer by layer. As we can see, constructing a feedback structure is an essential step to backpropagate the intermediate gradient signal from δ_k^{l+1} to δ_j^l , indicating that each weight of the feedback network must be brought into correspondence with the feed-forward network. (B): Predictive coding structure of SNN (PC-SNN). Both Predictions and prediction errors are updated in parallel mode using only local information. Note: Excitation denotes additive operator and Inhibition denotes subtraction operator.

threshold, it remains inactive. During training, it is essential to determine the firing times of all neurons. Therefore, if a neuron does not reach the threshold during training, its activation time is artificially set to the maximum time. And we followed the dynamic target firing time setting in S4NN (Kheradpisheh and Masquelier, 2020) which takes the actual activation time into account.

4.1.3. PC-SNN framework

To address the non-differentiable nature of SNNs and achieve local synaptic plasticity learning, we adopt predictive coding framework with inference and learning schemes inspired by the Expectation-Maximization (EM) algorithm (Dempster et al., 1977). The E-step involves finding the conditional expectation of the causes (inference), while the M-step determines the maximum likelihood value of the parameters (learning). As shown in Fig. 1(B), an SNN predictive coding model is presented alongside the BP-SNN architecture illustrated in Fig. 1(A).

Probabilistic Model: In the probabilistic point of view, we consider the firing time of IF neurons as a random variable. Let t^{l-1} be a vector of firing times on layer $l-1$, and t_j^l be the firing time of neuron j in layer l . Following the design of hierarchical models used in predictive coding (Friston, 2003), we assume

that adjacent layers' random variables satisfy the following relationships:

$$p(t_j^l | \mathbf{t}^{l-1}) = \mathcal{N}(t_j^l; \hat{t}_j^l, \Sigma_j^l) \quad (8)$$

where the mean probability density value \hat{t}_j^l is a non-linear function of lower-layer IF neuron activity and is determined as the moment when membrane potential $V_j^l(t)$ first crosses the threshold, with variance Σ_j^l remaining constant:

$$V_j^l(t) = \sum_i w_{ji}^l \sum_{\tau=1}^t \delta(\tau - t_i^{l-1}) \quad (9a)$$

$$\hat{t}_j^l = \min \{t : V_j^l(t) \geq \vartheta\} \quad (9b)$$

with a constant threshold ϑ and it is equal for all neurons in this work.

Inference: The E-step, also known as Inference, boosts the probability P based on the anticipated cause to achieve a reliable approximation of the recognition distribution indicated by network parameters. In this scenario, we use inference to identify the most probable random variable for neuron activity. To accomplish this, we must maximize the probability function given our inputs (for technical specifics, refer to (Friston, 2005)):

$$F = P(\mathbf{t}^1, \dots, \mathbf{t}^{l_{\max}} | \mathbf{t}^0) \quad (10)$$

to determine the activity of each IF neuron and converge F by iteratively modifying t_i^l values. To simplify the calculation, we express the probability function F in the form of the logarithm function (because of the monotonicity of the logarithm function, maximizing the logarithm function has the identical impact of maximizing the F function itself):

$$F = \ln(P(\mathbf{t}^1, \dots, \mathbf{t}^{l_{\max}} | \mathbf{t}^0)). \quad (11)$$

Since we assumed that the random variables on one layer depend only on that of the previous layer (first-order Markov property), we can rewrite the objective function as:

$$F = \sum_{l=1}^{l_{\max}} \ln(P(\mathbf{t}^l | \mathbf{t}^{l-1})). \quad (12)$$

Because the activity of each neuron in one layer is independent of each other, we can write the probability of the random variable vector as a product of single random variable probabilities. Substituting (8) and the expression for a normal distribution into the above equation (12), we obtain:

$$F = \sum_{l=1}^{l_{\max}} \sum_{j=1}^{n^l} \left[\ln \left(\frac{1}{\sqrt{2\pi}\Sigma_j^l} \right) - \frac{(t_j^l - \hat{t}_j^l)^2}{2\Sigma_j^l} \right] \quad (13)$$

where n^l represents the number of neurons in the l^{th} layer. Then, ignoring constant terms related to the variance, we can organize the objective function as

$$F = -\frac{1}{2} \sum_{l=1}^{l_{\max}} \sum_{j=1}^{n^l} \frac{(t_j^l - \hat{t}_j^l)^2}{\Sigma_j^l}. \quad (14)$$

To optimize the objective function mentioned above by determining the values of t_j^l , we can modify them proportionally to the gradient. When calculating the derivative of F with respect to t_j^l , we notice that each value affects F in two ways: it appears explicitly in (14), and it also impacts \hat{t}_k^{l+1} according to (9a). Therefore, the derivative consists of two terms:

$$\frac{\partial F}{\partial t_j^l} = -\frac{t_j^l - \hat{t}_j^l}{\Sigma_j^l} + \sum_{k=1}^{n^{l+1}} \frac{t_k^{l+1} - \hat{t}_k^{l+1}}{\Sigma_k^{l+1}} \cdot \frac{\partial \hat{t}_k^{l+1}}{\partial t_j^l}. \quad (15)$$

Let's denote

$$\varepsilon_j^l = (t_j^l - \hat{t}_j^l) / \Sigma_j^l \quad (16)$$

and this error node computes the difference between the current value of t_j^l and the mean of \hat{t}_j^l predicted by the lower layer. Then, from (15), we have:

$$\frac{\partial F}{\partial t_j^l} = -\varepsilon_j^l + \sum_{k=1}^{n^{l+1}} \varepsilon_k^{l+1} \cdot \frac{\partial \hat{t}_k^{l+1}}{\partial t_j^l}. \quad (17)$$

To compute the derivative $\frac{\partial \hat{t}_k^{l+1}}{\partial t_j^l}$, we unfold this term according to chain rule:

$$\frac{\partial \hat{t}_k^{l+1}}{\partial t_j^l} = \frac{\partial \hat{t}_k^{l+1}}{\partial V_k^{l+1}(t)} \cdot \frac{\partial V_k^{l+1}(t)}{\partial t_j^l}. \quad (18)$$

Assuming a small enough region around $t = \hat{t}_k^{l+1}$, we approximate the function $V_k^{l+1}(t)$ as a linear function of t for the first factor in (18) (Bohte et al., 2002). We denote the local derivative of $V_k^{l+1}(t)$ with respect to t as α , which is assumed to be a fixed positive constant in this paper. Since the threshold can only be reached on the rising edge of the membrane potential for the first time, it follows that $V_k^{l+1}(t)$ increases over time around $t = \hat{t}_k^{l+1}$. If there is an increment in $V_k^{l+1}(t)$ around $t = \hat{t}_k^{l+1}$, then intuitively, it will reach its threshold earlier and cause a decrease in firing time \hat{t}_k^{l+1} . Therefore, $\frac{\partial \hat{t}_k^{l+1}}{\partial V_k^{l+1}(t)} < 0$. To approximate $\frac{\partial \hat{t}_k^{l+1}}{\partial V_k^{l+1}(t)}$, considering the derivative of inverse function $V_k^{l+1}(t)$, we have:

$$\frac{\partial \hat{t}_k^{l+1}}{\partial V_k^{l+1}(t)} = -\frac{1}{\frac{\partial V_k^{l+1}(t)}{\partial t}} = -\frac{1}{\alpha}. \quad (19)$$

For the second factor in (18), it can be simplified by considering equation (9a). When t_j^l is reduced, $V_k^{l+1}(t)$ increases earlier in time by w_{kj}^{l+1} . Therefore, we can approximate $\frac{\partial V_k^{l+1}(t)}{\partial t_j^l}$ as $-w_{kj}^{l+1}$ only if $[t_j^l \leq \hat{t}_k^{l+1}]$. By substituting these derivative terms into equation (18), we obtain:

$$\frac{\partial \hat{t}_k^{l+1}}{\partial t_j^l} = \begin{cases} \frac{1}{\alpha} \cdot w_{kj}^{l+1} & \text{if } t_j^l \leq \hat{t}_k^{l+1} \\ 0 & \text{otherwise} \end{cases} \quad (20)$$

Finally, we have derived the following rule that describes how t_j^l changes over time:

$$\frac{\partial F}{\partial t_j^l} = -\varepsilon_j^l + \sum_{k=1}^{n^{l+1}} \varepsilon_k^{l+1} \cdot \frac{1}{\alpha} \cdot w_{kj}^{l+1} [t_j^l \leq \hat{t}_k^{l+1}] \quad (21)$$

and the temporal activity t_j^l is updated depending only on local nodes and weights.

Learning parameters: In the inference section, we set the firing time of neurons on the highest layer to match the target output firing time ($t_i^o = T_i^o$). The firing times of all neurons on layer $l \in \{1, \dots, l_{\max} - 1\}$ are adjusted using the same method as before (see Eq. (21)). From a neurobiological perspective, both learning and inference aim to minimize free energy F in exactly the same way according to Friston's theory (Friston, 2005). As we modify w_{kj}^{l+1} proportionally to its objective function gradient, our network gradually approaches a steady state. Eventually, updating all synaptic weights will lead to predicting desired outputs. It should be noted that modifying w_{kj}^{l+1} affects \hat{t}_k^{l+1} and thus influences function value F formulated in (14):

$$\begin{aligned} \frac{\partial F}{\partial w_{kj}^{l+1}} &= \frac{t_k^{l+1} - \hat{t}_k^{l+1}}{\Sigma_k^{l+1}} \cdot \frac{\partial \hat{t}_k^{l+1}}{\partial w_{kj}^{l+1}} \\ &= \varepsilon_k^{l+1} \cdot \frac{\partial \hat{t}_k^{l+1}}{\partial V_k^{l+1}(t)} \cdot \frac{\partial V_k^{l+1}(t)}{w_{kj}^{l+1}} \\ &= \varepsilon_k^{l+1} \cdot -\frac{1}{\alpha} \cdot \sum_{\tau=1}^{\hat{t}_k^{l+1}} S_j^l(\tau) \end{aligned} \quad (22)$$

where $\sum_{\tau=1}^{\hat{t}_k^{l+1}} S_j^l(\tau) = 1$ if $t_j^l \leq \hat{t}_k^{l+1}$ else 0.

According to (21) and (22), the change in neuron activity t_j^l and synaptic weight w_{kj}^{l+1} between layer l and $l+1$ are both proportional to the product of temporal quantities encoded on these two adjacent layers, which can be directly obtained by local connection. The update of its weight (w_{kj}^{l+1}) depends only on temporal activities of presynaptic and postsynaptic nodes, i.e., ε_k^{l+1} and $S_j^l(t)$, satisfying biologically-plausible local plasticity. This is in contrast to the expression of backpropagation, where the weight changes depending on intermediate variables that are passed from the back to the front through a complex function of activities and weights. We refer to the changes in (22) as local Hebbian synaptic plasticity in a manner that the weight change is a simple product of temporal activities of presynaptic and postsynaptic spiking neurons. We use pseudocode to describe the learning and prediction process in Algorithm 1 and Algorithm 2, respectively.

4.1.4. PC-SNN analysis

We assume that the dataset $\mathcal{Z} = (\mathcal{X}, \mathcal{Y})$ is complete, but only \mathcal{X} is observed. In this context, we consider an input spike $S^0(t)$ and a target firing time T^o as \mathcal{X} , which is given. The latent variables \mathbf{t}^l on layer $l \in \{1, \dots, l_{\max} - 1\}$ are considered as \mathcal{Y} . We denote the complete-data log likelihood by $l(\theta; \mathcal{X}, \mathcal{Y})$, where θ represents the unknown parameter vector for which we want to find the Maximum Likelihood Expectation. Here, $l(\theta; \mathcal{X}, \mathcal{Y})$ corresponds to our objective function F , following a nonlinear model under Gaussian assumptions (Equation (8)). The parameter set of the spiking neural network is denoted by θ . According to Bishop's EM algorithm (Bishop and Nasrabadi, 2006), one has following steps:

E-Step: The E-step of the EM algorithm computes the expected value of $l(\theta; \mathcal{X}, \mathcal{Y})$ given the observed

data \mathcal{X} , and the current parameter estimate θ_{old} . In particular, we define:

$$\begin{aligned} F(\theta; \theta_{old}) &:= \mathbb{E}[l(\theta; \mathcal{X}, \mathcal{Y}) \mid \mathcal{X}, \theta_{old}] \\ &= \int l(\theta; \mathcal{X}, y) p(y \mid \mathcal{X}, \theta_{old}) dy \end{aligned} \quad (23)$$

where $p(\mathcal{Y} \mid \mathcal{X}, \theta_{old})$ is the conditional density of \mathcal{Y} given the observed data, \mathcal{X} . The goal of the E-step is to determine the distribution of $p(\mathcal{Y} \mid \mathcal{X}, \theta_{old})$, which can also be defined as Gaussian. In the present context of the hierarchical Gaussian generative model, we define $p(\mathcal{Y} \mid \mathcal{X}, \theta_{old}) = \prod_1^{l_{max}-1} \mathcal{N}(\mathcal{Y}^l; \mu^l, \sigma^l)$, $l = 1 : l_{max} - 1$. This intractable posterior can be approximated with variational inference as proved in (Millidge et al., 2020). The final updating form of neural activities in (Millidge et al., 2020) coincides with maximizing $F(\theta; \theta_{old})$ with respect to θ in the inference process, as shown in (17).

M-Step: The M-step consists of maximizing over θ the expectation computed in (23), that is, we set:

$$\theta_{new} := \max_{\theta} F(\theta; \theta_{old}). \quad (24)$$

Then, we set $\theta_{old} = \theta_{new}$ for iteration updating. This solution of M-step is shown as the parameters updated in (22). The two steps are repeated as necessary until the sequence of θ_{new} 's converges.

Algorithm 1: Learning with predictive coding

```

for all training Data do
  Temporal coding:  $\mathbf{S}^0 \leftarrow \mathbf{S}^{input}$ ;
  Setting dynamic target firing time:  $\mathbf{t}^{l_{max}} \leftarrow \mathbf{T}^o$ ;
  while not convergence do
    Inference:
     $\varepsilon_i^l = \frac{t_i^l - \hat{t}_i^l}{\Sigma_i^l}$ ;
     $\hat{t}_i^l = -\varepsilon_i^l + \sum_{j=1}^{n^{l+1}} \varepsilon_j^{l+1} \cdot \frac{1}{\alpha} \cdot w_{ji}^{l+1} [t_i^l \leq \hat{t}_j^{l+1}]$ ;
     $t_i^l \leftarrow t_i^l + \hat{t}_i^l$ ;
    Update weights:
     $\dot{w}_{ji}^{l+1} = \varepsilon_j^{l+1} \cdot -\frac{1}{\alpha} \cdot \sum_{\tau=1}^{\hat{t}_j^{l+1}} S_i^l(\tau)$ ;
     $w_{ji}^{l+1} \leftarrow w_{ji}^{l+1} + \eta \dot{w}_{ji}^{l+1}$ ;
  end
end

```

Algorithm 2: Prediction after training

```

for all testing Data do
  Temporal coding:  $\mathbf{S}^0 \leftarrow \mathbf{S}^{input}$ ;
  Forward pass to compute predictions:
   $V_j^l(t) = \sum_i w_{ji}^l \sum_{\tau=1}^t S_i^{l-1}(\tau)$ ;
   $t_j^l = \min \{t : V_j^l(t) \geq \vartheta\}$ ;
end

```

4.2. ASRNN

4.2.1. ASRNN for regression

Yin et al. (2021) demonstrate that state-of-the-art performance for sequential and temporal tasks in SNNs is attainable through the use of an Adaptive Spiking Recurrent Neural Network, which is capable of learning temporal dynamics. This is achieved using a new substitute differential, the Gaussian distribution, in backpropagation. The results are comparable to conventional RNNs, with a theoretical energy advantage of 1 to 3 orders of magnitude. This advantage grows with task complexity, requiring larger networks for precise solutions. Theoretically, the ASRNN model supports long-term and short-term memory, analogous to LSTM and other traditional neural network memory units. In this paper, the ASRNN is extended to continuous-time regression prediction for the first time, improving upon the previous SRM-based model. Originating from the LIF spiking neuron, Adaptive SRNN integrates input current $I(t)$ in a leaky manner and fires an action potential when its membrane potential $\mu(t)$ crosses a dynamic threshold θ . The threshold increases after each spike and decays exponentially with time constant τ_{adp} . The differential equation is expressed as follows:

$$\tau_m \frac{d\mu}{dt} = -\mu(t) + R_m I(t) - \tau_m \theta(t) S(t) \quad (25)$$

$$\tau_{adp} \frac{d\theta}{dt} = -(\theta(t) - b_0) + \beta S(t) \quad (26)$$

In simulation, the continuous neuron model is discretized, we set the time interval as $dt = 1ms$, combined with the first-order Taylor expansion, The n_l layer feed-forward spiking convolutional neural network based on ASRNN is modeled as follows:

$$s^0(t) = s_{in}(t) \quad (27a)$$

$$\eta^{l+1}(t) = \rho \eta^{l+1}(t-1) + (1-\rho) s^{l+1}(t-1) \quad (27b)$$

$$\vartheta^{l+1}(t) = b_0 + \beta \eta^{l+1}(t) \quad (27c)$$

$$I^{l+1}(t) = W^{l+1} s^l(t) \quad (27d)$$

$$u^{l+1}(t) = \alpha u^{l+1}(t-1) + (1-\alpha) R_m I^{l+1}(t) - \vartheta^{l+1}(t) s^{l+1}(t-1) \quad (27e)$$

$$s^l(t) = \sum \delta(t - t^f) \quad (27f)$$

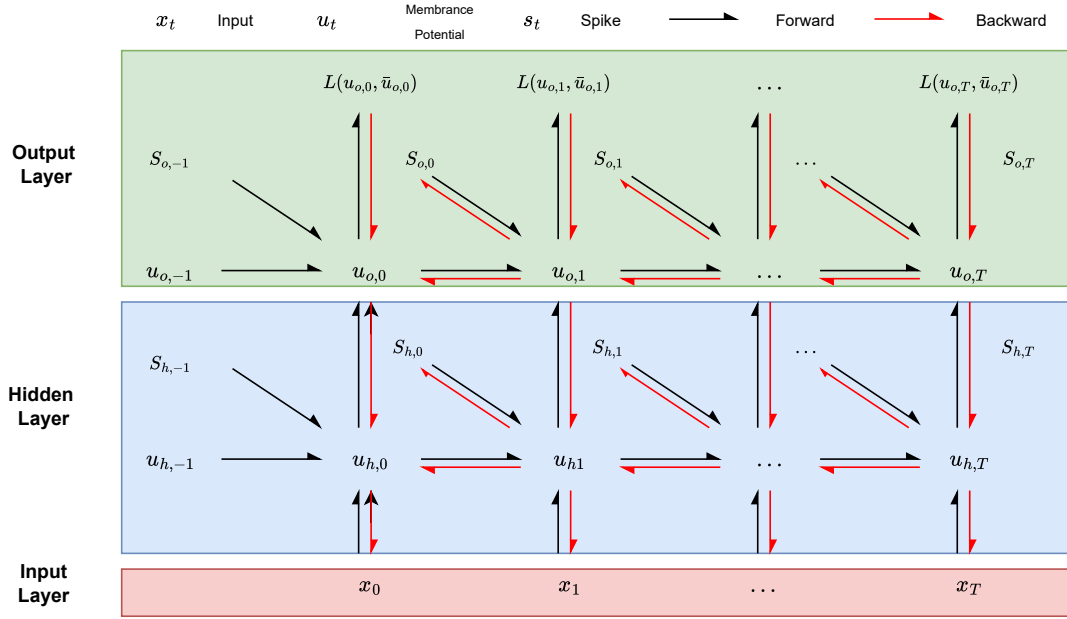
$$t^f \in \{t \mid u^l(t) = \vartheta\} \quad (27g)$$

$$\omega(t) = u^o(t) \quad (27h)$$

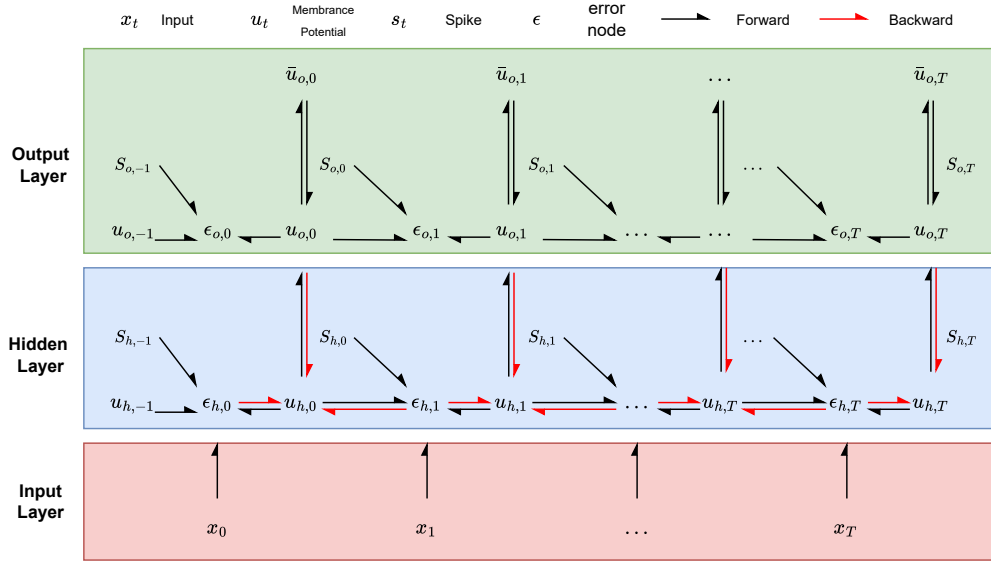
where $\alpha = \exp(-dt/\tau_m)$ is the single-timestep decay of the membrane potential with time-constant τ_m , $\rho = \exp(-dt/\tau_{adp})$ is the single-timestep decay of the threshold with time-constant τ_{adp} , ϑ is a dynamical threshold comprised of a fixed minimal threshold b_0 and an adaptive contribution $\beta\eta$; The parameter β is a constant that controls the size of adaptation of the threshold.

4.2.2. ASRNN-BPTT Algorithm

In this section, we derive the ASRNN-BPTT algorithm and analyze the derivation results. By BPTT, the difference between the prediction and target is transmitted from the output layer back to the input



(a) ASRNN-BPTT



(b) ASRNN-PCTT

Figure 2: An diagram illustration between ASRNN-BPTT and ASRNN-PCTT.

layer, including the input layer at the past time, optimizing weights and parameters by gradient descent. Conceptually, BPTT expands the network at all input time steps.

The discontinuous nature in spiking neurons makes it difficult to apply the chain rule to calculate the back propagation gradient. In practice, replacing discontinuous gradients with surrogate gradients, has been shown to be effective, making it possible to implement spiking neural networks training on mainstream deep learning frameworks such as PyTorch and Tensorflow. A variety of alternative gradient functions were

proposed and evaluated, including multi-Gaussian function, Gaussian function, linear function and SLayer function. For these functions, however, the study showed no significant difference in performance. We use Gaussian function (Yin et al., 2020) in this paper: $\hat{f}'_s(u_t) = \mathcal{N}(u_t | \theta, \sigma^2)$.

In the event camera angular velocity prediction task, we need to generate an output at each step t . The loss function L is defined as the Euclidean distance of the predicted angular velocity $\omega(t)$ and the ground truth angular velocity $\bar{\omega}(t)$ over time:

$$L = \frac{1}{T_1 - T_0} \int_{T_0}^{T_1} \sqrt{e(t)^\top e(t)} dt \quad (28)$$

where $e(t) = \omega(t) - \bar{\omega}(t)$. The loss function estimates the prediction error of angular velocity in the whole simulation time, i.e. 100ms with a time step of 1ms. So the discretized form of the loss function is obtained:

$$L = \frac{1}{T_1 - T_0} \sum_{t=T_0}^{T_1} L(t) \quad (29a)$$

$$L(t) = \|\mathbf{u}^o(t) - \bar{\mathbf{u}}^o(t)\| \quad (29b)$$

By the chain rule, We get the derivative of the loss function with respect to the weight w_{ji}^{l+1} :

$$\frac{\partial L}{\partial w_{ji}^{l+1}} = \sum_{t=T_0}^{T_1} \frac{\partial L(t)}{\partial w_{ji}^{l+1}} = \sum_{t=T_0}^{T_1} \frac{\partial L(t)}{\partial \mu_j^{l+1}(t)} \cdot \frac{\partial \mu_j^{l+1}(t)}{\partial w_{ji}^{l+1}} \quad (30)$$

For the first derivative term in the right side of (30), we denote the error term as:

$$\delta_j^{l+1}(t) = \frac{\partial L(t)}{\partial \mu_j^{l+1}(t)} = \sum_{k=1}^{n^{l+2}} \frac{\partial L(t)}{\partial \mu_k^{l+2}(t)} \cdot \frac{\partial \mu_k^{l+2}(t)}{\partial \mu_j^{l+1}(t)}$$

where $\frac{\partial \mu_k^{l+2}(t)}{\partial \mu_j^{l+1}(t)} = (1 - \alpha) R_m w_{kj}^{l+2} \hat{f}'_s(u_j^{l+1}(t))$ according to spiking neuron model depicted in (27e). Therefore, the recursive calculation of the error term from the output layer to the current layer is obtained:

$$\delta_j^{l+1}(t) = (1 - \alpha) \hat{f}'_s(u_j^{l+1}(t)) \sum_{k=1}^{n^{l+2}} \delta_k^{l+2}(t) w_{kj}^{l+2} \quad (31)$$

For the second derivative term in the right side of (30), it is necessary to go through all time steps before t and calculate iteratively in time as follows:

$$\frac{\partial \mu_j^{l+1}(t)}{\partial w_{ji}^{l+1}} = (1 - \alpha) s_i^l(t) + \frac{\partial u_j^{l+1}(t)}{\partial u_j^{l+1}(t-1)} \cdot \frac{\partial u_j^{l+1}(t-1)}{\partial w_{ji}^{l+1}}$$

Denote $\lambda_j^{l+1}(t) = \frac{\partial u_j^{l+1}(t)}{\partial u_j^{l+1}(t-1)}$, and the gradient backtracking of BPTT from the current time step t to the

previous time step can be obtained as follows:

$$\frac{\partial \mu_j^{l+1}(t)}{\partial w_{ji}^{l+1}} = (1 - \alpha)s_i^l(t) + \lambda_j^{l+1}(t) \cdot \frac{\partial u_j^{l+1}(t-1)}{\partial w_{ji}^{l+1}} \quad (32)$$

The calculation graph is shown in Fig. 2(a). As shown, the calculation of weight gradient requires backpropagating in both spatial and temporal dimensions. Specifically, the error term $\delta_j^{l+1}(t)$ needs to be propagated layer by layer from the output layer as (31), and the iterative gradient $\frac{\partial u_j^{l+1}(t)}{\partial w_{ji}^{l+1}}$ also needs to be calculated recursively from initial time step as (32). On the one hand, spatial backpropagation of the error term $\delta_j^{l+1}(t)$ uses too much global information, i.e. the activity of neurons that are not directly connected to the weight modified, instead of local information, thus does not satisfy the local plasticity in biology. On the other hand, backpropagation through time is a common phenomenon in recurrent neural networks, which may cause problems such as gradient explosion or gradient vanishing.

4.2.3. ASRNN-PCTT Algorithm

In order to further improve the BPTT algorithm mentioned above, inspired by Predictive Coding theory in (Rao and Ballard, 1999; Friston, 2003, 2005; Whittington and Bogacz, 2017), we propose a new supervised learning algorithm, ASRNN-PCTT, and apply it to a dataset for predicting angular velocity in event cameras.

Probabilistic Model We regard membrane potential of neurons as random variable in the probabilistic point of view, and assume that the random variables on adjacent layers satisfies the following relationships:

$$P(u_i^l(t) | \mathbf{u}^{l-1}(t)) = \mathcal{N}(u_i^l(t); \hat{u}_i^l(t), \Sigma_i^l) \quad (33)$$

where the mean value of probability distribution $\hat{u}_i^l(t)$ satisfies the following expression according to original Adaptive SRNN neuron model in (27e):

$$\hat{u}_i^l(t) = \alpha u_i^l(t-1) + (1 - \alpha) R_m \sum_h w_{ih}^l s_h^{l-1}(t) - s_i^l(t-1) \theta_i^l(t) \quad (34)$$

Inference Given the spiking input from the event-camera, Inference process is to find the most likely neuron activity random variable. We need to maximize the probability function:

$$F = \prod_{t=T_0}^{T_1} P(\mathbf{u}^1(t), \dots, \mathbf{u}^{l_{\max}}(t) | \mathbf{u}^0(t))$$

Converting objective function F into logarithmic form, and the joint probability distribution is decomposed into products of probabilities, F can be written as :

$$F = -\frac{1}{2} \sum_{t=T_0}^{T_1} \sum_{l=1}^{l_{\max}} \sum_{i=1}^{n^l} \frac{(u_i^l(t) - \hat{u}_i^l(t))^2}{\Sigma_i^l} \quad (35)$$

In calculating the derivative of the objective function (35) with respect to $u_i^l(t)$, it is observed that each random variable $u_i^l(t)$ affects the objective function in three ways. First, it appears explicitly in the formula (35); Second, it implicitly influences objective function by affecting $\hat{u}_i^l(t)$; Third, it also affects the objec-

tive function by affecting $\hat{u}_i^l(t+1)$, as (34). Therefore, the derivative of the objective function with respect to $u_i^l(t)$ contains the following three items:

$$\frac{\partial F}{\partial u_i^l(t)} = -\varepsilon_i^l(t) + \sum_{j=1}^{n^{l+1}} \varepsilon_j^{l+1}(t) \cdot \frac{\partial \hat{u}_j^{l+1}(t)}{\partial u_i^l(t)} + \varepsilon_i^l(t+1) \frac{\partial \hat{u}_i^l(t+1)}{\partial u_i^l(t)} \quad (36)$$

where the local error node $\varepsilon_i^l(t)$ computes the difference between the current value of $u_i^l(t)$ and the mean value $\hat{u}_i^l(t)$ that predicted by the lower layers:

$$\varepsilon_i^l(t) = \frac{u_i^l(t) - \hat{u}_i^l(t)}{\Sigma_i^l}$$

In addition, denote $\lambda_i^l(t+1) = \frac{\partial \hat{u}_i^l(t+1)}{\partial u_i^l(t)}$ and infer that $\frac{\partial \hat{u}_j^{l+1}(t)}{\partial u_i^l(t)} = (1-\alpha)R_m w_{ji}^{l+1} \hat{f}'_s(u_i^l(t))$, the derivative of the objective function with respect to $u_i^l(t)$ can be summarized as follows:

$$\begin{aligned} \frac{\partial F}{\partial u_i^l(t)} = & -\varepsilon_i^l(t) + \sum_{j=1}^{n^{l+1}} \varepsilon_j^{l+1}(t) \cdot (1-\alpha)R_m w_{ji}^{l+1} \hat{f}'_s(u_i^l(t)) \\ & + \varepsilon_i^l(t+1) \lambda_i^l(t+1) \end{aligned} \quad (37)$$

Learning parameters In the Inference section, the random variable of the neurons on the output layer are set to the target angular velocity, i.e. $\mathbf{u}^o(t) = \bar{\mathbf{u}}^o(t)$. The values of random variable of all neurons on layer l ($l \in \{1, \dots, l_{\max} - 1\}$) and time t ($t \in \{T_0, \dots, T_1\}$) are adjusted in the way as (37) for several steps until convergence. After that, the network parameter w_{ji}^{l+1} is updated with information in steady state. Easy to see that the weight w_{ji}^{l+1} affects the value of the objective function F by influencing the mean of probability model, i.e. $\hat{u}_j^{l+1}(t)$, and we get:

$$\frac{\partial F}{\partial w_{ji}^{l+1}} = \sum_{t=T_0}^{T_1} \varepsilon_j^{l+1}(t) \cdot (1-\alpha)R_m s_i^l(t) \quad (38)$$

The calculation graph of PCTT is shown in Fig. 2(b). According to (37) and (38), it can be concluded that whether the update of membrane potential or the update of weight parameters, in terms of spatial network structure, only local error nodes and weight information directly adjacent to the modified quantity are involved. In terms of time, it only utilizes the error nodes of the current time or next time step. More importantly, these error nodes do not need to be calculated recursively in time, but exist in the calculation graph during inference, and can thus realize asynchronous calculation. Compared to the BPTT algorithm in Fig. 2(a), PCTT algorithm does not require a separate feedback network in both spatial dimension and time domain. This local and asynchronous property of this algorithm may engender a promising prospect of more efficient implementations on neuromorphic hardware and may also facilitate the development of fully distributed neuromorphic architectures. Moreover, it also provides a new idea for solving the problem of gradient explosion/vanishing in BPTT.

5. Experiments

5.1. Experimental Setup

5.1.1. Datasets

We selected three datasets for our experiments: Caltech 101 and MNIST for object classification tasks, and an event camera-based dataset for angular velocity regression. The Caltech101 Face/Motorbike Dataset is a publicly available classification dataset that includes various images of faces and motorbikes. The MNIST dataset is a common benchmark for image classification tasks, comprising 60,000 training images and 10,000 test images. Each image displays a handwritten digit ranging from 0 to 9 and has dimensions of 28×28 pixels. The CIFAR-10 dataset (Krizhevsky et al., 2009) is a collection of 60,000 32×32 color images in 10 classes, with 6,000 images per class. The Event Camera Angular Velocity Dataset is an open-source synthetic dataset (Gehrig et al., 2020), which uses ESIM (Rebecq et al., 2018) as the event camera simulator. This dataset matches DAVIS240C Event-camera with a resolution of 240×180 and selects 10000 panoramic images from a sub-set of Sun360 dataset (Xiao et al., 2012). The random rotational motion used to generate this data covers all axes evenly, resulting in uncorrelated angular velocities across the entire dataset with a mean value of zero.

5.1.2. Implementation Details

For the Caltech101 Face/Motorbike dataset, we implemented a PC-SNN with a network architecture of $28 \times 50 - 200 - 2$. The output layer consists of two Integrate-and-Fire (IF) neurons, each representing either a face or a motorbike. We initialized the weights of both the hidden and output layers randomly from uniform distributions within the ranges $[0, 1]$ and $[0, 5]$, respectively. For the MNIST dataset, we employed a PC-SNN with a size of $28 \times 28 - 200 - 10$ that used first-spike temporal coding in the input layer with maximum simulation time $t_{max} = 256$. We varied the variance of the hidden and output layers in our probabilistic model ($\Sigma^{(1)} = 10, \Sigma^{(2)} = 20$) and set learning rates for the hidden and output layers at $\eta = 0.06$ and $\eta = 0.02$ respectively. The threshold for membrane potential was set at 100, while the distance term in target firing time was $\gamma = 20$. Synapse weights were randomly initialized from uniform distributions ranging between $[0, 5]$ and $[0, 10]$ for the two different layers. To further demonstrate the effectiveness of our method on a large-scale classification dataset, We evaluated our method on CIFAR-10 based on the VGG-11 and VGG-16 network structure, and the other parameters align with MNIST dataset, all details are shown in Table 1. For the angular velocity regression task, the spiking convolutional neural network is composed of five convolutional layers, a spiking global pooling layer, and a fully connected layer, which outputs the predicted angular velocity values in three dimensions: tilt, pan, and roll. The first four convolutional layers use a step size of 2 to perform spatial downsampling. Starting with 16 channels in the first convolutional layer, the number of channels in each subsequent convolutional layer is doubled. Shallow feature extraction module parameters remain frozen, while fully connected layer parameters are updated. To balance computation time and performance, the number of inferences was set to 5. In our simulation, we set $T_0 = 0\text{ms}$, $T_1 = 100\text{ms}$, $dt = 1\text{ms}$, and the rest parameters were set in Table 2.

5.2. Evaluation Metrics

To measure the classification performance of SNNs, we employ the following accuracy metric: the percentage of correctly classified instances by the model. For the quantitative evaluation of regression performance, the criteria used in the event camera angular velocity prediction experiment include the following two measures:

Table 1: Model parameters setting for PC-SNN

Dataset	Model Parameters					
	t_{max}	ϑ	γ	α	η	Σ
Caltech	256	100	8	1	0.1	10
MNIST	256	100	20	1	[0.06,0.02]	10
CIFAR-10	256	100	20	1	[0.1,0.06,0.02]	10

Table 2: Model parameters setting for ASRNN

Method	Model Parameters							
	b_0	R_m	β	τ_m	τ_{adp}	Σ	lr	
ASRNN-based BPTT	0.1	6	2.0	4	700	-	2e-3	
ASRNN-based PCTT	0.1	6	2.0	4	700	10	2e-4	

(1) Root mean Square Error (RMSE)

$$RMSE = \frac{1}{T_1 - T_0} \int_{T_0}^{T_1} \sqrt{\mathbf{e}(t)^\top \mathbf{e}(t)} dt \quad (39)$$

(2) Relative error

$$R_e = \frac{\|\omega(t) - \bar{\omega}(t)\|}{\|\bar{\omega}(t)\|} \quad (40)$$

5.3. Experimental Results

5.3.1. Classification

For classification task, we run our PC-SNN algorithm on two different public image classification datasets to evaluate the local compute predictive coding block. Experiments and analysis are performed to compare our method with other non-convoluted spike-based method. Our experiment goal is to demonstrate the predictive coding block is able to achieve comparable performance levels and simultaneously provides the advantages of biological plausibility and local computation in the same time. We evaluated our PC-SNN method on the Caltech face/motorcycle dataset. Detailed results are shown in Table. 3. Our PC-SNN method achieved 99.3% top-1 accuracy, surpassing existing SNN method. Second, we evaluated our method on the MNIST dataset, where the PC-SNN achieved state-of-the-art performance of 98.1%, compared to other SNN methods. Finally, we evaluated our method on the CIFAR-10 dataset, where the PC-SNN achieved comparable performance of 92.51%, compared to other SNN methods. Details are shown in Table. 3.

For verify and analyze the functionalities of the proposed PC-SNN, we investigated the membrane potential of output neurons, i.e., V_i^o after training. As depicted in Fig. 3, we present the classification results of four sample colored images with the proposed PC-SNN. Each of the colored images was first resized

Table 3: Comparison of the Classification Accuracy of Different SNN Models on the Caltech face/motorcycle, MNIST and CIFAR-10 datasets

Dataset	Method	Network Architecture	Coding	Neuron model	Acc. (%)
Caltech face/motorcycle	R-STDP (Mozafari et al., 2018b)	-	Temporal	Rectified linear	98.2
	SDNN (Kheradpisheh et al., 2018)	-	Temporal	LIF	99.1
	S4NN (Kheradpisheh and Masquelier, 2020)	-	Temporal	IF	99.2
	STiDi-BP (Mirsadeghi et al., 2021)	-	Temporal	linear SRM	99.2
	SSTDP (Liu et al., 2021a)	-	Temporal	IF	99.3
	PC-SNN(Ours)	-	Temporal	IF	99.3
MNIST	BP-STDP (Tavanaei and Maida, 2019)	784FC-1000FC-10FC	Rate	IF	96.6
	S4NN (Kheradpisheh and Masquelier, 2020)	784FC-400FC-10FC	Temporal	IF	97.4
	STiDi-BP (Mirsadeghi et al., 2021)	40C5-P2-1000FC-10FC	Temporal	linear SRM	99.2
	SSTDP (Liu et al., 2021a)	784FC-300FC-10FC	Temporal	IF	98.1
	PC-SNN(Ours)	784FC-200FC-10FC	Temporal	IF	98.1
CIFAR10	SPIKE-NORM (Sengupta et al., 2019)	VGG-16	Rate	IF	91.55
	PTL (Wu et al., 2021)	VGG-11	Rate	IF	91.24
	T2FSNN (Park et al., 2020)	VGG-16	Temporal	LIF	91.43
	SSTDP (Liu et al., 2021a)	VGG-7	Temporal	IF	91.31
	TSC (Han and Roy, 2020b)	VGG-16	Temporal	IF	93.63
	LC-TTFC (Yang et al., 2023)	VGG-11	TTFS	ReL-PSP	91.25
	LC-TTFC (Yang et al., 2023)	VGG-16	TTFS	ReL-PSP	92.72
	PC-SNN(Ours)	VGG-11	Temporal	IF	91.29
PC-SNN(Ours)	VGG-16	Temporal	IF	92.51	

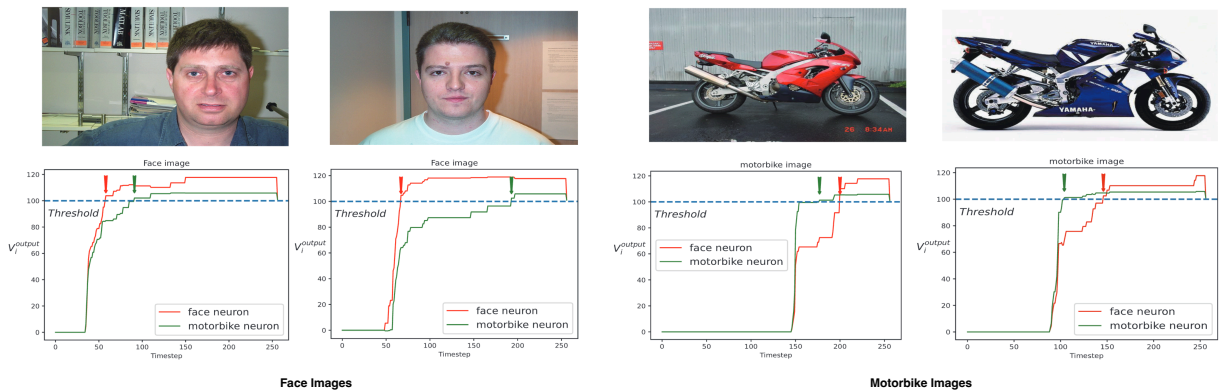


Figure 3: Temporal membrane potentials of output neurons over some Caltech101 face/motorbike images. Arrows indicate the firing time of the corresponding output neuron.

into 28×50 pixels and converted into grayscale before encoding using TTFS coding strategy. Then, with the pixel density of grayscale and 28×50 input neurons, the TTFS technique encodes each image into binary spike train consisting of only zeros and ones. In this coding scheme, the initial spike activation time of each neuron is determined by the magnitude of the pixel density. Greater pixel values correspond

to earlier emission times. After integration of the spike trains of the hidden layer, the corresponding two output neurons' membrane potentials are in the time interval of $[0, t_{max}]$.

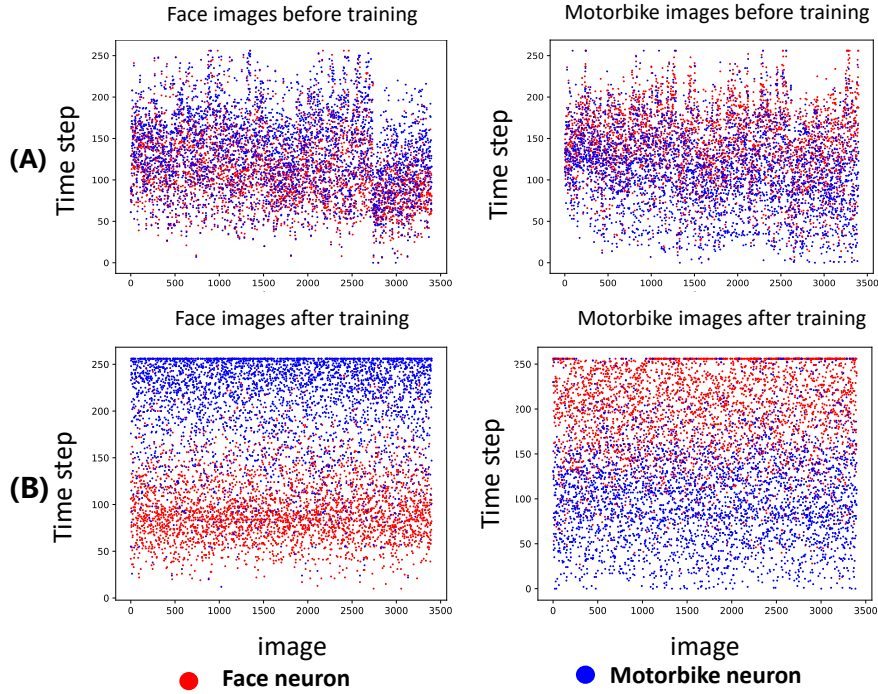


Figure 4: Scatter of firing time of two output neurons on Face/Motorbike images at different stages.(A) Before training; (B) After training.

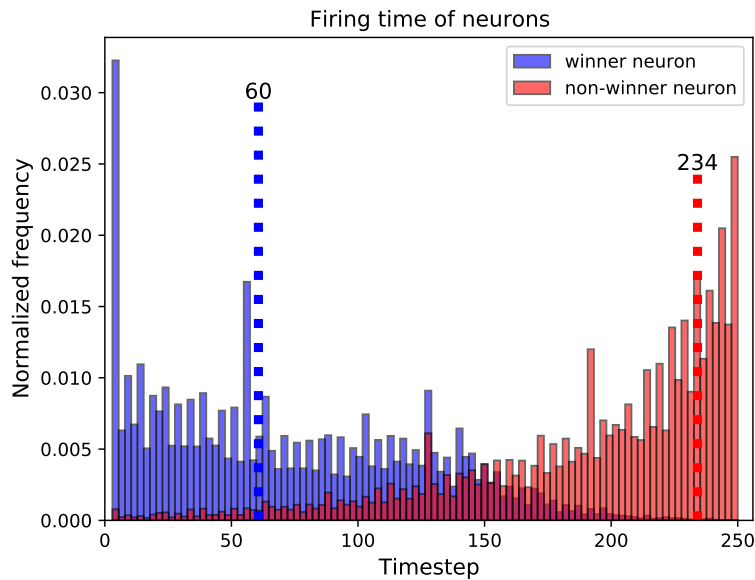


Figure 5: The histogram of the firing time for the winner neurons(blue bar) and non-winner neurons(red bar) over the training images. The dashed line indicates the mean firing time of the winner(non-winner) neuron.

For every sample image, the target neuron's membrane potential grows faster and reaches the threshold

earlier than that of another neuron. In Fig. 4, we investigated the firing time distribution of the face and motorbike output neurons over 3600 face and 3600 motorbike images at A) the beginning and B) the end of the learning process. As we can see, the firing time of the two output neurons before training was disordered, indicating that the spiking neuron network was not capable of classification at this time. After training, the neuron corresponding to the correct category fired significantly earlier than the other. Some neurons gather at t_{max} because if they are not activated within a set time interval, their firing time is artificially set to t_{max} . Fig. 5 shows the firing time distribution of the winner neuron (earliest activated neuron) and non-winner neurons. About 90% of winner neurons activate before 150 timesteps, with an average firing time of 60 timesteps. In contrast, 85% of non-winner neurons fire after 150 timesteps, with an average of 234 timesteps. This clear separation aids network training and judgment, with PC-SNN responding to input images within about 60 timesteps 50% of the time. Fig. 6 shows the convergence speed of the PC-SNN, SSTDP (Liu et al., 2021a), and S4NN (Kheradpisheh and Masquelier, 2020) on the MNIST dataset. As demonstrated, the PC-SNN converges faster than the SSTDP and S4NN.

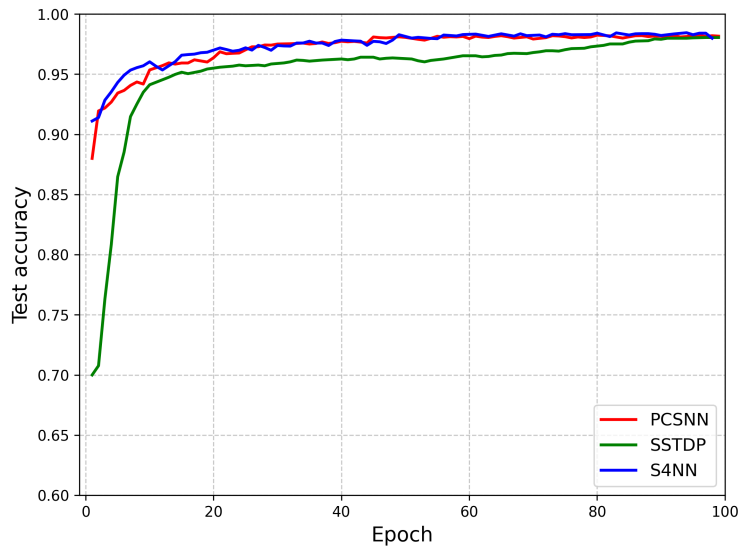


Figure 6: Comparison of MNIST test accuracy convergence over 100 epochs for three SNN models: PCSNN, SSTDP, and S4NN.

5.3.2. Regression

For the regression task, we explored the applicability of ASRNN to predict angular velocity of a rotating event camera. We compared existing methods to our ASRNN method trained using either BPTT or PCTT. The performance comparison of several baseline models are listed in Table 4. The spiking convolutional network structure of the SRM-BP algorithm (Gehrig et al., 2020) is the same in this work. ANN-6 is a 6-layer convolutional neural network using ReLU as the activation function, and "V" indicates Voxel-Grid events. The input event type used by the ResNet-50 algorithm is "A," which represents the two-channel frames calculated through accumulating events, while "E" represents the original events from the event cameras. The prediction gap between the baseline obtained by the ResNet-50 and ANN-6 architectures is due to differences in their input representations. Unlike the Voxel-based method, the Accumulation-based method discards the time of the event completely. This significantly influences the performance of continuous-time regression prediction of angular velocity.

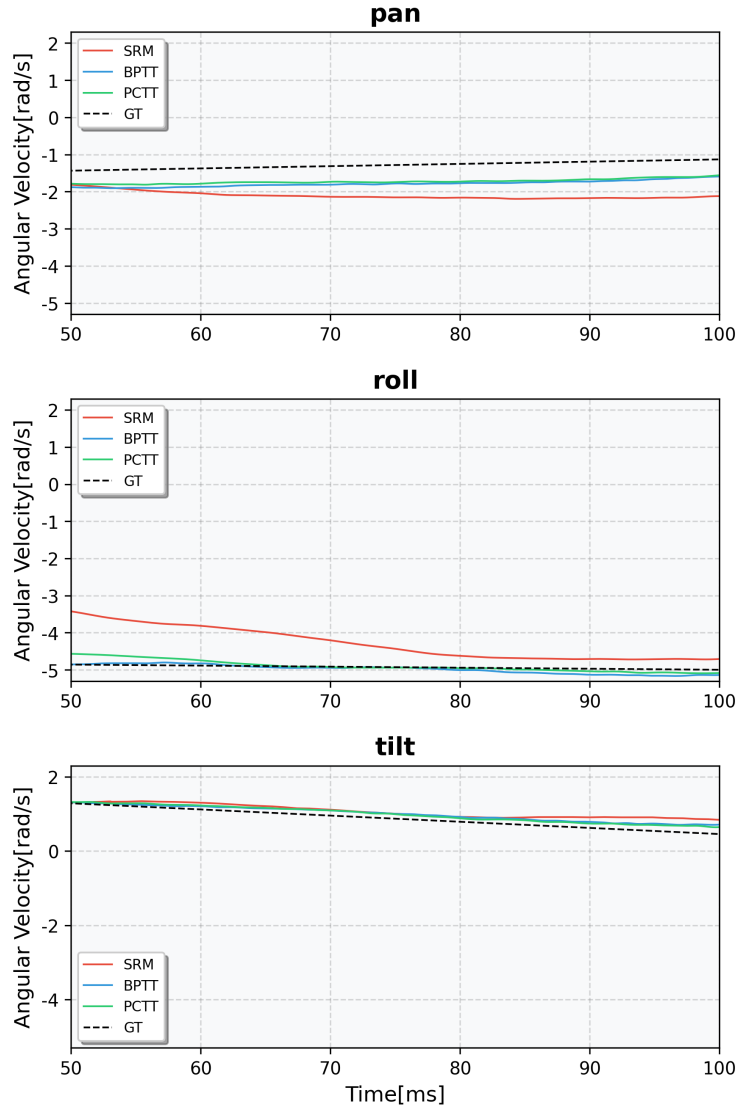


Figure 7: Continuous-time angular velocity predictions by three algorithms (SRM, BPTT, PCTT) and the corresponding ground truth.

ASRNN-Based BPTT Algorithm proposed in this paper achieves better performance compared with the previous work – SRM-based backpropagation algorithm: Our relative error is 0.22 and RMSE is 60.39 deg/s, which improves the RMSE by 6 deg/s compared with the previous SRM model, and is better than the Accumulation-based ResNet-50 algorithm. At the same time, this result is comparable to the result of Voxel-Based ANN-6 algorithm. Moreover, in our method, the event-based input does not need any preprocessing, it really realizes the end-to-end angular velocity prediction. The RMSE obtained by the PCTT algorithm is 59.58 deg/s and Relative error is 0.22, which is closer to the current ANN best result of 59.0 deg/s. This may be attributed to the elimination of iteration in time, solving the possible problem of gradient explosion or vanishing in BPTT. In addition, PCTT has the advantage of biological feasibility and satisfies the local plasticity in biological neurology.

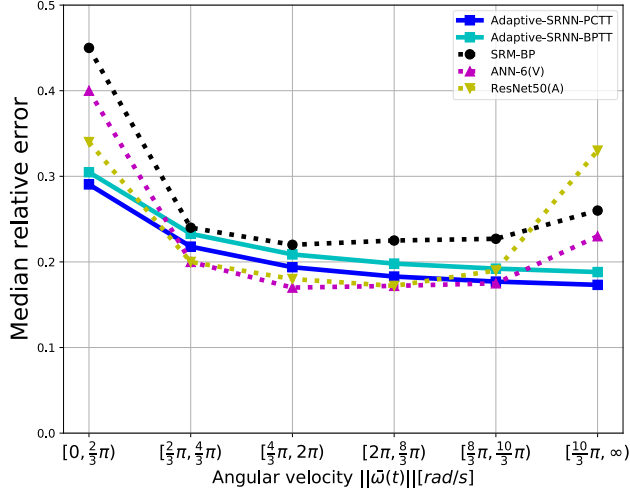


Figure 8: Median relative Error of all baseline models in different angular velocity ranges of the test set

Table 4: Event Camera Angular Velocity

Method	Input Type	Relative error	RMSE (deg/s)
ANN-6	V	0.22	59.0
ResNet-50	A	0.22	66.8
SRM-BP (Gehrig et al., 2020)	E	0.26	66.3
ASRNN-BPTT	E	0.22	60.39
ASRNN-PCTT	E	0.22	59.58

V indicates that Voxel-Grid event

A indicates two-channel frames calculated through accumulating events

E indicates the original events

We illustrate the 50 - 100ms continuous-time angular velocity prediction of random sample of ASRNN-based BPTT algorithm and PCTT algorithm in Fig. 7. Compared with SRM-based algorithm, it can be concluded from qualitative analysis that the ASRNN-based algorithm can achieve more accurate predictions. The predicted angular velocity in three directions can all well track the ground truth angular velocity, and the error between the predicted value and the ground truth is smaller than SRM-based algorithm. Fig. 8 and Table 4 illustrate the median relative errors of all baseline models. At low angular velocities, all models exhibit relatively high errors (0.3), with ASRNN-based BPTT (0.31) and PCTT (0.29) outperforming other baselines. At high angular velocities, our proposed methods achieve errors below 0.2. For intermediate velocities, our methods perform comparably to ANN-6 (A) and ResNet-50 (V), with median relative errors of approximately 0.22. Overall, the proposed ASRNN-based approaches demonstrate superior performance at both low and high angular velocity ranges.

5.4. Time Complexity Analysis

The time complexity of PC-SNN for training K-layer SNNs with biologically plausible algorithms offers the advantage of lower algorithmic complexity. We denote the computational costs of one-step feedforward and one-step local-plasticity propagation as n and m , respectively. PC-SNN completes the feedforward step

at a cost of $O(nK)$, where K is the number of layers. It then performs parallel inference across all hidden layers using local information and updates the network parameters for each layer in a local-plasticity manner, also in parallel. Thus, the algorithm complexity is $O(nK + 2mK)$. In contrast, BP-SNN not only incurs a feedforward cost of $O(nK)$ but also involves multistep backpropagation layer by layer using differential chain rule with computing cost of $O(nK + (m + mK)K)$ (Zhang et al., 2021). The PC-SNN algorithm updates spiking temporal activities and weights using only information from directly connected nodes, allowing for parallel implementation. This local and parallelizable property makes our algorithm a promising candidate for more efficient implementations on neuromorphic hardware. It may also facilitate the development of fully distributed neuromorphic architectures.

5.5. Biological Plausibility

Learning in the brain occurs through changes in synaptic connections between neurons, and there is very limited evidence suggesting that exact formulations of backpropagation exist in the cortex. Despite SNN’s biological plausibility nature, primarily learning methods still align with traditional AI, neglecting its brain-like learning mechanisms and biological plausibility. Our PC-SNN framework relies on a Hebbian-based rule to regulate synaptic plasticity, controlled entirely by local nodes which shares similarities with synaptic plasticity in the human brain (Lillicrap et al., 2020; Caucheteux et al., 2023; Lillicrap et al., 2016).

6. Conclusion and Discussion

Our work implement the predictive coding learning framework to spiking neural networks for image and event camera rotation datasets, using only local information and end-to-end training. The results are comparable to state-of-the-art SNN learning methods, showcasing the framework’s capabilities in SNN training. The proposed networks are evaluated on three images datasets and one event camera datasets: Caltech Face/Motorbike, MNIST, CIFAR10 and event camera angular velocity dataset. Our proposed framework offers two prominent features: (1) Biological plausibility is achieved by using only local information in both the inference and weight update process. PC-SNN eliminates the need for a separate feedback network, processing information asynchronously and concurrently in a parallel, local manner. (2) Our proposed learning rule suits on-chip learning perfectly due to lower wiring layout complexity derived from elimination of feedback network. Although hardware implementation is beyond scope of this paper, we believe that our model provides research potential on hardware implementation in an energy-efficient manner.

References

- Aceituno, P. V., Farinha, M. T., Loidl, R., and Grewe, B. F. (2023). Learning cortical hierarchies with temporal hebbian updates. *Frontiers in Computational Neuroscience*, 17:1136010.
- Bengio, Y. and Fischer, A. (2015). Early inference in energy-based models approximates back-propagation. *Computer Science*.
- Bi, G.-q. and Poo, M.-m. (1998). Synaptic modifications in cultured hippocampal neurons: dependence on spike timing, synaptic strength, and postsynaptic cell type. *Journal of neuroscience*, 18(24):10464–10472.
- Bishop, C. M. and Nasrabadi, N. M. (2006). *Pattern recognition and machine learning*, volume 4. Springer.

- Bohte, S. M., La Poutre, J. A., and Kok, J. N. (2002). Error-backpropagation in temporally encoded networks of spiking neurons. *Error-backpropagation in temporally encoded networks of spiking neurons*, 48(1-4):17–37.
- Caucheteux, C., Gramfort, A., and King, J.-R. (2023). Evidence of a predictive coding hierarchy in the human brain listening to speech. *Nature Human Behaviour*, 7(3):430–441.
- Crick and Francis (1989). The recent excitement about neural networks. *Nature*, 337(6203):129–132.
- Dempster, A. P., Laird, N. M., and Rubin, D. B. (1977). Maximum likelihood from incomplete data via the em algorithm. *Journal of the royal statistical society: series B (methodological)*, 39(1):1–22.
- Friston, K. (2003). Learning and inference in the brain. *Neural Networks*, 16(9):1325–1352.
- Friston, K. (2005). A theory of cortical responses. *Philosophical transactions of the Royal Society B: Biological sciences*, 360(1456):815–836.
- Gehrig, M., Shrestha, S. B., Mouritzen, D., and Scaramuzza, D. (2020). Event-based angular velocity regression with spiking networks. In *2020 IEEE International Conference on Robotics and Automation (ICRA)*, pages 4195–4202. IEEE.
- Guo, Y., Zhang, L., Chen, Y., Tong, X., Liu, X., Wang, Y., Huang, X., and Ma, Z. (2022). Real spike: Learning real-valued spikes for spiking neural networks. In *European Conference on Computer Vision*, pages 52–68. Springer.
- Han, B. and Roy, K. (2020a). Deep spiking neural network: Energy efficiency through time based coding. In *European conference on computer vision*, pages 388–404. Springer.
- Han, B. and Roy, K. (2020b). Deep spiking neural network: Energy efficiency through time based coding. In *European conference on computer vision*, pages 388–404. Springer.
- Han, B., Srinivasan, G., and Roy, K. (2020). Rmp-snn: Residual membrane potential neuron for enabling deeper high-accuracy and low-latency spiking neural network. In *Proceedings of the IEEE/CVF conference on computer vision and pattern recognition*, pages 13558–13567.
- Jiang, H., Anumasa, S., De Masi, G., Xiong, H., and Gu, B. (2023). A unified optimization framework of ann-snn conversion: towards optimal mapping from activation values to firing rates. In *International Conference on Machine Learning*, pages 14945–14974. PMLR.
- Kheradpisheh, S. R., Ganjtabesh, M., Thorpe, S. J., and Masquelier, T. (2018). Stdp-based spiking deep convolutional neural networks for object recognition. *Neural Networks*, 99:56–67.
- Kheradpisheh, S. R. and Masquelier, T. (2020). Temporal backpropagation for spiking neural networks with one spike per neuron. *International journal of neural systems*, 30(06):2050027.
- Krizhevsky, A., Hinton, G., et al. (2009). Learning multiple layers of features from tiny images.
- Li, Y., Deng, S., Dong, X., Gong, R., and Gu, S. (2021). A free lunch from ann: Towards efficient, accurate spiking neural networks calibration. In *International conference on machine learning*, pages 6316–6325. PMLR.

- Li, Y., Kim, Y., Park, H., Geller, T., and Panda, P. (2022). Neuromorphic data augmentation for training spiking neural networks. In *European Conference on Computer Vision*, pages 631–649. Springer.
- Lillicrap, T. P., Cownden, D., Tweed, D. B., and Akerman, C. J. (2016). Random synaptic feedback weights support error backpropagation for deep learning. *Nature Communications*, 7(1):13276.
- Lillicrap, T. P., Santoro, A., Marris, L., Akerman, C. J., and Hinton, G. (2020). Backpropagation and the brain. *Nature Reviews Neuroscience*, 21(6):335–346.
- Lin, F. (2021). Supervised learning in neural networks: Feedback-network-free implementation and biological plausibility. *IEEE Transactions on Neural Networks and Learning Systems*, pages 1–11.
- Liu, F., Zhao, W., Chen, Y., Wang, Z., Yang, T., and Jiang, L. (2021a). Sstdp: Supervised spike timing dependent plasticity for efficient spiking neural network training. *Frontiers in Neuroscience*, 15:756876.
- Liu, F., Zhao, W., Chen, Y., Wang, Z., Yang, T., and Li, J. (2021b). Sstdp: Supervised spike timing dependent plasticity for efficient spiking neural network training. *Frontiers in neuroscience*, page 1413.
- Maass, W. (1997). Networks of spiking neurons: the third generation of neural network models. *Neural networks*, 10(9):1659–1671.
- Millidge, B., Tschantz, A., and Buckley, C. L. (2020). Predictive coding approximates backprop along arbitrary computation graphs. *arXiv preprint arXiv:2006.04182*.
- Mirsadeghi, M., Shalchian, M., Kheradpisheh, S. R., and Masquelier, T. (2021). Stidi-bp: Spike time displacement based error backpropagation in multilayer spiking neural networks. *Neurocomputing*, 427:131–140.
- Mostafa, H. (2017). Supervised learning based on temporal coding in spiking neural networks. *IEEE transactions on neural networks and learning systems*, 29(7):3227–3235.
- Mozafari, M., Kheradpisheh, S. R., Masquelier, T., Nowzari-Dalini, A., and Ganjtabesh, M. (2018a). First-spike-based visual categorization using reward-modulated stdp. *IEEE transactions on neural networks and learning systems*, 29(12):6178–6190.
- Mozafari, M., Kheradpisheh, S. R., Masquelier, T., Nowzari-Dalini, A., and Ganjtabesh, M. (2018b). First-spike-based visual categorization using reward-modulated stdp. *IEEE transactions on neural networks and learning systems*, 29(12):6178–6190.
- Ororbias, A. and Mali, A. (2023). Convolutional neural generative coding: Scaling predictive coding to natural images.
- Ororbias, A., Mali, A., Kohan, A., Millidge, B., and Salvatori, T. (2024). A review of neuroscience-inspired machine learning. *arXiv preprint arXiv:2403.18929*.
- Park, S., Kim, S., Na, B., and Yoon, S. (2020). T2fsnn: deep spiking neural networks with time-to-first-spike coding. In *2020 57th ACM/IEEE design automation conference (DAC)*, pages 1–6. IEEE.
- Rao, R. P. and Ballard, D. H. (1999). Predictive coding in the visual cortex: a functional interpretation of some extra-classical receptive-field effects. *Nature neuroscience*, 2(1):79–87.

- Rathi, N., Srinivasan, G., Panda, P., and Roy, K. (2020). Enabling deep spiking neural networks with hybrid conversion and spike timing dependent backpropagation. *arXiv preprint arXiv:2005.01807*.
- Rebecq, H., Gehrig, D., and Scaramuzza, D. (2018). Esim: an open event camera simulator. In *Conference on robot learning*, pages 969–982. PMLR.
- Roy, K., Jaiswal, A., and Panda, P. (2019). Towards spike-based machine intelligence with neuromorphic computing. *Nature*, 575(7784):607–617.
- Salvatori, T., Mali, A., Buckley, C. L., Lukasiewicz, T., Rao, R. P., Friston, K., and Ororbia, A. (2023). Brain-inspired computational intelligence via predictive coding. *arXiv preprint arXiv:2308.07870*.
- Sengupta, A., Ye, Y., Wang, R., Liu, C., and Roy, K. (2019). Going deeper in spiking neural networks: Vgg and residual architectures. *Frontiers in neuroscience*, 13:95.
- Song, Y., Lukasiewicz, T., Xu, Z., and Bogacz, R. (2020). Can the brain do backpropagation?—exact implementation of backpropagation in predictive coding networks. *Advances in neural information processing systems*, 33:22566.
- Summerfield, C., Egner, T., Greene, M., Koechlin, E., Mangels, J., and Hirsch, J. (2006). Predictive codes for forthcoming perception in the frontal cortex. *Science*, 314(5803):1311–1314.
- Summerfield, C., Trittschuh, E. H., Monti, J. M., Mesulam, M.-M., and Egner, T. (2008). Neural repetition suppression reflects fulfilled perceptual expectations. *Nature neuroscience*, 11(9):1004–1006.
- Tavanaei, A. and Maida, A. (2019). Bp-stdp: Approximating backpropagation using spike timing dependent plasticity. *Neurocomputing*, 330:39–47.
- Whittington, J. C. and Bogacz, R. (2017). An approximation of the error backpropagation algorithm in a predictive coding network with local hebbian synaptic plasticity. *Neural computation*, 29(5):1229–1262.
- Wu, J., Xu, C., Han, X., Zhou, D., Zhang, M., Li, H., and Tan, K. C. (2021). Progressive tandem learning for pattern recognition with deep spiking neural networks. *IEEE Transactions on Pattern Analysis and Machine Intelligence*, 44(11):7824–7840.
- Xiao, J., Ehinger, K. A., Oliva, A., and Torralba, A. (2012). Recognizing scene viewpoint using panoramic place representation. In *2012 IEEE conference on computer vision and pattern recognition*, pages 2695–2702. IEEE.
- Yang, Q., Zhang, M., Wu, J., Tan, K. C., and Li, H. (2023). Lc-ttfs: Toward lossless network conversion for spiking neural networks with ttfs coding. *IEEE Transactions on Cognitive and Developmental Systems*, 16(5):1626–1639.
- Yao, M., Zhao, G., Zhang, H., Hu, Y., Deng, L., Tian, Y., Xu, B., and Li, G. (2023). Attention spiking neural networks. *IEEE transactions on pattern analysis and machine intelligence*.
- Yin, B., Corradi, F., and Bohté, S. M. (2020). Effective and efficient computation with multiple-timescale spiking recurrent neural networks. In *International Conference on Neuromorphic Systems 2020*, pages 1–8.

- Yin, B., Corradi, F., and Bohté, S. M. (2021). Accurate and efficient time-domain classification with adaptive spiking recurrent neural networks. *Nature Machine Intelligence*, 3(10):905–913.
- Zenke, F. and Ganguli, S. (2018). Superspike: Supervised learning in multilayer spiking neural networks. *Neural computation*, 30(6):1514–1541.
- Zhang, T., Jia, S., Cheng, X., and Xu, B. (2021). Tuning convolutional spiking neural network with biologically plausible reward propagation. *IEEE Transactions on Neural Networks and Learning Systems*, 33(12):7621–7631.
- Zipser, D. and Rumelhart, D. E. (1993). The neurobiological significance of the new learning models. In *Computational neuroscience*, pages 192–200.